Nano Research

Open Access

Research Article

Synthesis of multi-element (F,N,S) doped carbon nanospheres derived from polystyrene as lubricant additives for tribological performance improvement

Yixin Wang[1], Yi Wang[1], Yuhong Cui[1], Sha Liu[1], Shujuan Liu[1], Qian Ye[1] ✉, Feng Zhou[1,2] ✉, and Weimin Liu[1,2]

[1] *State Key Laboratory of Solidification Processing, Center of Advanced Lubrication and Seal Materials, School of Materials Science and Engineering, Northwestern Polytechnical University, Xi'an 710072, China*
[2] *State Key Laboratory of Solid Lubrication, Lanzhou Institute of Chemical Physics, Chinese Academy of Sciences, Lanzhou 730000, China*

Cite this article: *Nano Research*, **2025**, *18*, 94906995. https://doi.org/10.26599/NR.2025.94906995

ABSTRACT: In this study, the uniform dense polydopamine (PDA) coating was deposited on hyper-cross-linked polystyrene nanospheres (HPSs) through the oxidative polymerization of dopamine with polyethyleneimine (PEI), then which underwent acidification and subsequent anion exchange with $LiNTf_2$ to obtain HPSs@PDA electrolyte (HPSs@PDA-NTf_2). So, the multi-element-doped carbon nanospheres (F,N,S-PCNs) were synthesized through the carbonization of HPSs@PDA-NTf_2, demonstrating exceptional tribological performance. Compared to 500SN, the mean COF of nanolubricant (500SN + 2.0 wt.% F,N,S-PCNs) decreased from 0.181 to 0.110, and the wear volume reduced by 90.3%. The load-carrying capacity of F,N,S-PCNs as lubricant additives is increased from 150N (500SN) to 450N. The F,N,S-PCNs can infiltrate the contact area and adsorb on the friction pair surface, forming a physical adsorption film that prevents the direct contact of surface. Additionally, the active elements (F,N,S) in F,N,S-PCNs undergo tribochemical reactions with the friction pair under mechanical force and thermal effects to form a chemical protective film. This dual effect significantly enhances the boundary lubrication performance of the lubricating oil. This study presents a novel approach for synthesizing multi-element co-doped carbon nanospheres, significantly enhancing the effectiveness of oil-based lubrication technology in the field.

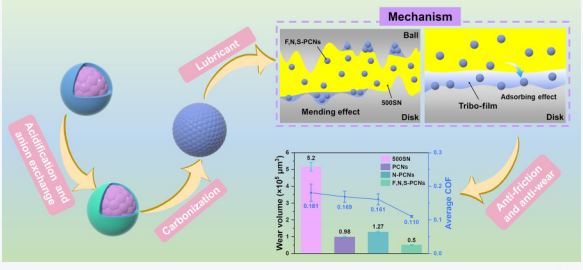

KEYWORDS: carbon nanospheres, surface modification, element doping, lubricant additives, tribological behavior

1 Introduction

In the operation of mechanical equipment, friction is unavoidable and can lead to material degradation, energy dissipation, equipment failure, and environmental pollution [1, 2]. Lubrication technology has been developed to reduce friction and prolong the operational lifespan of mechanical equipment [3]. This technology primarily involves forming a lubricating film between contacting surfaces, with the aim of minimizing frictional forces and reducing wear. Developing new lubricant formulations to achieve energy efficiency is a key scientific task due to the performance limitations of existing lubricants in various fields. Due to their unique physicochemical characteristics, nanoparticles such as metal [4], metal oxides [5], metal sulfides [6], carbon nanoparticles [7], nanocomposites [8] have been widely studied and employed as additives in the past few years [9]. However, these nanomaterials tend to agglomerate in base oil due to themselves high surface energy, which hinders the achievement of optimal lubrication efficiency.

For decades, carbon materials (including graphene [10], carbon nanotubes [11], nanodiamonds [12], and amorphous carbon [13], among other variants) have been extensively studied in the fields of tribology due to their diverse forms, excellent corrosion resistance, outstanding mechanical properties, and high thermal conductivity [14–16]. Liu et al. have developed a three-dimensional (3D) graphene additive with tribological properties. When incorporated into base oil, it can reduce the friction coefficient (COF) by 22% and wear rate by 95% [10]. Additionally, Zhang et al. synthesized a kilogram-scale of carbon dots (CDs) as a nano-additive, achieving a substantial 75% reduction in the COF [17]. The rich and well-established chemistry of carbon nanostructures offers endless opportunities for properties tuning compared to other types of

Received: July 16, 2024; **Revised:** August 19, 2024
Accepted: August 20, 2024

✉Address correspondence to Qian Ye, yeqian213@nwpu.edu.cn; Feng Zhou, zhouf@licp.cas.cn

nanomaterials [18, 19]. These heteroatoms, such as fluorine (F), nitrogen (N), phosphorus (P), sulfur (S), and selenium (Se), can be individually or collectively incorporated into carbon frameworks through the carbonization of heteroatom-rich precursors [20]. These heteroatoms have the ability to adjust the physical and chemical properties of carbon, enhance its interaction with lubricants, and improve its capability to form a protective film on steel substrates [21]. Jin et al successfully synthesized N,S co-doped carbon dots via laser treatment of heterocyclic aromatic hydrocarbons, which exhibit outstanding anti-friction properties (reducing the COF from 0.650 to 0.093) and exceptional anti-wear properties (reducing wear volume by 92.0%) as a lubrication additive [22]. Wang et al. fabricated amorphous carbon films co-doped with F and S, achieving an exceptionally low steady-state COF of 0.01–0.02 [23]. By means of controlled pyrolysis, polymers can be converted into carbon materials with precise structures. In comparison to traditional small molecular hydrocarbons, polymers as carbon sources provide superior manipulation over the total number of carbon and doped atoms, essential for creating carbon materials with specific doping characteristics [24]. Additionally, spherical nanoparticles demonstrate high load-bearing capacity and extreme pressure characteristics in various tribological applications due to their ball bearing effect in friction studies [9]. Polydopamine (PDA), polymerized from dopamine under mildly alkaline conditions, has the ability to create a PDA layer on different types of nanomaterials [25]. Notably, PDA exhibits zwitterionic properties with an isoelectric pH around 4.0. Due to these zwitterionic properties [26, 27], PDA can undergo ion exchange to form a PDA electrolyte [28].

Herein, we have developed dense and stable PDA coating on hyper-cross-linked polystyrene nanospheres (HPSs) through the oxidative polymerization of dopamine, assisted by polyethyleneimine (PEI) in a pH 8.5 Tris(hydroxymethyl)-aminomethane (Tris) aqueous solution. The resulting PDA film undergoes acidification and subsequent anion exchange with $LiNTf_2$ to produce HPSs@PDA electrolyte (HPSs@PDA-NTf_2). These were then carbonized at 400 °C to prepare multi-element doping of carbon nanospheres (F,N,S-PCNs). Due to their small size, the as-prepared F,N,S-PCNs effectively penetrate the contact area and generate a positive lubricating effect. Driven by van der Waals forces, the adsorption of F,N,S-PCNs on the friction pair surface directly reduces friction in the boundary lubrication state and protects the surfaces from direct contact. The adsorbed nanoparticles with active elements (F,N,S) undergo friction-induced chemical reactions under mechanical force and thermal energy, significantly improving the boundary lubrication performance of the lubricant, this improvement is evidenced by a reduced COF to 0.110 and a 90.3% reduction in wear volume.

2 Experimental section

2.1 Materials

Potassium persulfate (AR), dopamine hydrochloride (98%), divinyl benzene (80%), styrene (AR), ethylene imine polymer (M_W 10,000, 99%) and bis(trifluoromethane)sulfonimide lithium salt ($LiNTf_2$, 98%) are obtained from TCI. Acetone (AR), hydrochloric (AR), and ethyl alcohol (AR) are purchased from Aladdin. Tris (AR, 99%) is acquired from Chemical Reagent Company of Shanghai (Shanghai, China).

2.2 Preparation of polydopamine-modified HPSs (HPSs@PDA)

The preparation methodology for polystyrene nanospheres (PS) and HPSs remains consistent with our prior research [29]. The HPSs (200 mg) and dopamine hydrochloride (80 mg) were weighed and uniformly dispersed in 10 mL of anhydrous ethanol; Disperse 80 mg of PEI in 20 mL of Tris aqueous solution. Recombine the two aforementioned solutions at room temperature and stir for 24 h. Upon completion of the reaction, the sample underwent washing with water and ethanol to obtain the HPSs@PDA. The detailed preparation procedure is depicted in Scheme 1.

2.3 Preparation of HPSs@PDA-NTf_2 and F,N,S-PCNs

Disperse 150 mg of HPSs@PDA in 20 mL of an aqueous solution, and adjust the pH of the solution to 4 using 0.1 M HCl. Add 30 mL

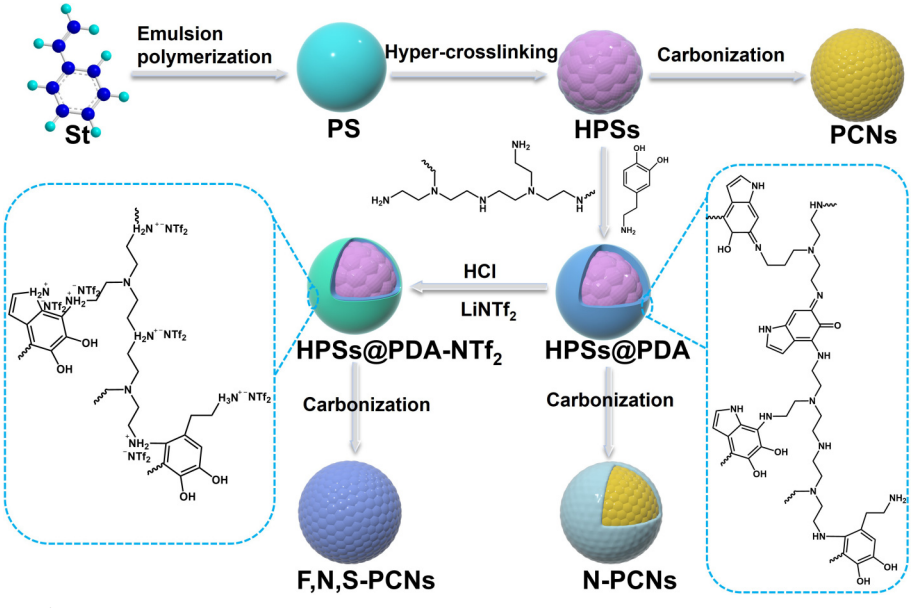

Scheme 1 Schematic diagram of preparation F,N,S-PCNs.

of ethyl acetate into the aforementioned dispersion solution. Disperse 28.7 g of $LiNTf_2$ in 10 mL of an aqueous solution and incorporate it into the aforesaid mixture, while vigorously stirring for a duration of 24 h. After the completion of the reaction, the sample is rinsed with water to obtain the HPSs@PDA-NTf_2 [28]. The PCNs, N-PCNs, and F,N,S-PCNs were obtained at 400 °C after 3 h of carbonization treatment for HPSs, HPSs@PDA, and HPSs@PDA-NTf_2, respectively (Scheme 1).

3 Results and discussions

Scanning electron microscopy (SEM) and transmission electron microscopy (TEM) facilitate the investigation into the structure and properties of materials to explore the microscopic characteristics. After undergoing carbonization treatment, the PCNs retain their exceptional spherical structure (Fig. S1 in the Electronic Supplementary Material (ESM)). A significant contrast difference is manifested for the oxygen elements between the surface and interior of HPSs@PDA, which is attributed to the formation of a polymer coating via Michael addition and Schiff base reaction between PEI and polydopamine on HPSs' surface (Fig. 1). After the ion exchange with NTf_2^-, new sulfur and fluorine signals were detected in the HPSs@PDA-NTf_2. Owing to the presence of the surface coating, HPSs@PDA-NTf_2 retains its distinctive core–shell structure (Fig. 1 and Fig. S2 in the ESM). The distribution of oxygen elements in N-PCNs mirrors that of HPSs@PDA. This similarity is attributed to the incomplete decomposition of the PDA layer at 400 °C. The distribution of O, F, N and S in the F,N,S-PCNs exhibited homogeneity, indicating that F, N and S were integrated into the carbon nanospheres during carbonizing HPSs@PDA-NTf_2 (Fig. 1 and Fig. S2 in the ESM). As revealed by the TEM results of F,N,S-PCNs, the core–shell structure of HPSs@PDA-NTf_2 vanishes after undergoing high-temperature carbonization, which may contribute to an augmented cracking of PDA-NTf_2, resulting in almost complete carbonization of the PDA-NTf_2 coating.

The zeta potential serves as a crucial parameter for elucidating the surface characteristics of nanospheres. The zeta potential of the HPSs (−17.8 mV) was enhanced to 32.5 mV for HPSs@PDA and 43.3 mV for HPSs@PDA-NTf_2 (Fig. S3 in the ESM), conclusively validating the successful completion of Michael addition/Schiff base reaction, and decoration of PDA-NTf_2 electrolyte. After undergoing high-temperature carbonization, the surface potentials of PCNs, N-PCNs, and F,N,S-PCNs were measured as −0.2, 11.7, and 18.1 mV,

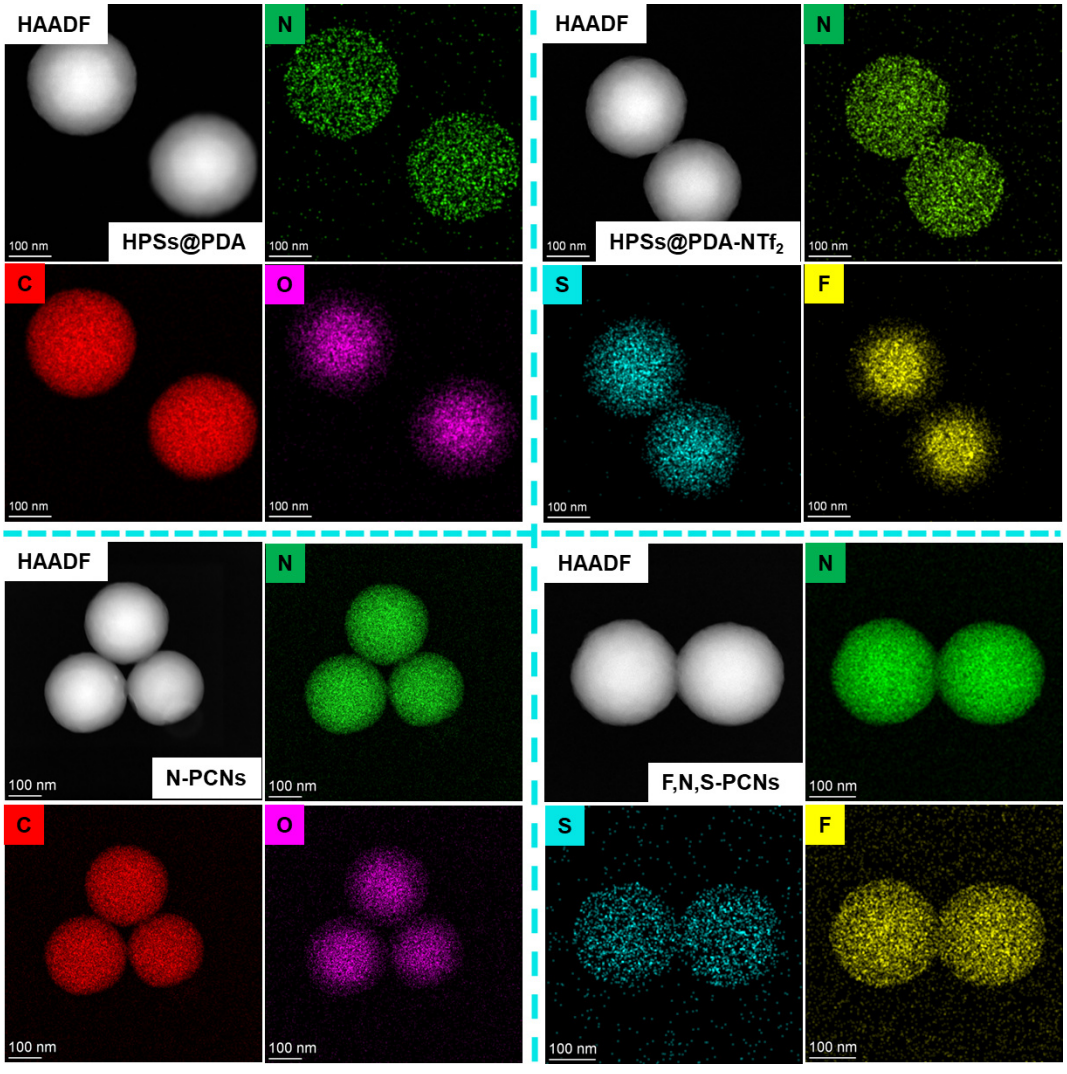

Figure 1 High-angle annular dark field (HAADF) image and energy dispersive X-ray spectroscopy (EDS) mapping of HPSs@PDA, HPSs@PDA-NTf_2, N-PCNs and F,N,S-PCNs.

respectively (Fig. 2(a)). The chemical constituents of the samples are elucidated via Fourier transform infrared spectroscopy (FT-IR) spectra (Fig. S4 in the ESM and Fig. 2(b)). The adsorption peaks at 2854 and 2923 cm^{-1} in the HPSs@PDA are associated with the stretching vibrations of the C–H and C=C inherent to the indole structures (Fig. S4 in the ESM) [28]. The adsorption peaks observed at 1602 and 1513 cm^{-1} correspond to the bending and shearing vibrations of N–H, confirming the existence of imine and amine moieties within the PDA units [28]. The peak observed at 1700 cm^{-1} is due to the formation of C=N bond between PDA and PEI [25]. The HPSs@PDA-NTf_2 spectrum exhibits new absorption peaks at 1346 and 1056 cm^{-1}, due to the stretching vibrations of S=O and C–F, respectively, which further confirms the successful grafting of PDA-NTf_2 electrolyte. The N-PCNs exhibit new absorption peaks at 850 (N–H), 1090 (C–N), 1445 (C–N), and 1600 (C=N) cm^{-1}, providing evidence of successful nitrogen doping in the carbon nanosphere [30–32]. Compared with N-PCNs, F,N,S-PCNs exhibit new absorption peaks at 600, 1185, and 1240 cm^{-1}, owing to C–S, C–S/C–N/C–O, and O=S=O stretching vibrations, respectively, which confirm the successful sulfur doping into the carbon nanosphere [33, 34]. The results depicted in Fig. 2(c) and Fig. S5 in the ESM indicate the emergence of new N and F signals in HPSs@PDA-NTf_2 and F,N,S-PCNs. The sulfur signals are prominently detected in the X-ray photoelectron spectroscopy (XPS) high-resolution spectrum and the doping concentration of S element in F,N,S-PCNs is 0.6 at.%. (Fig. 2(d) and Table S1 in the ESM). The peaks observed at 164.0 and 168.5 eV in the S $2p_{3/2}$ spectrum are assigned to the C–S–C and C–SO_3–H bonds, respectively [35]. The high-resolution C 1s XPS spectra of N-PCNs (Fig. 2(e)) exhibit distinct peaks at 284.8 (C–C), 286.3 (C–O/C–N), and 288.8 eV (C=O). The high-resolution C 1s XPS spectra of F,N,S-PCNs exhibited novel binding energy at 291.5 eV (C–F_2), corresponding to the fine spectrum of F 1s (687.5 and 688.8 eV) (the doping concentration of F is 4.3 at.%) (Fig. 2(f)) [36, 37]. Compared to N-PCNs (399.6 eV for C–N), the novel peaks attributed to pyridinic-N (398.9 eV) and pyrrolic-N (400.8 eV) emerged in the fine spectrum of F,N,S-PCNs (Fig. 2(g)). Moreover, the nitrogen content of F,N,S-PCNs increases to 4.6 at.% compared to the 1.3 at.% in N-PCNs (Table S1 in the ESM). Thermogravimetric (TG) analysis is a pivotal analytical technique that quantifies the mass change of materials as they undergo controlled heating, enabling precise determination of their thermal properties and compositional characteristics. Based on Fig. 2(h), it is evident that PCNs, N-PCNs, and F,N,S-PCNs demonstrate significant thermal decomposition at temperatures exceeding 400 °C. Furthermore, the thermal stability of F,N,S-PCNs (the mass loss is 18.5 wt.%) surpasses that of PCNs (the mass loss is 38.6 wt.%) and N-PCNs (the mass loss is 44.2 wt.%) notably when the temperature reaches 800 °C. The N_2 adsorption–desorption isotherm depicted in Fig. S6 in the ESM demonstrates a significant uptake of N_2 at low pressures (relative pressure P/P_0 = 0–0.1), indicating the presence of a distinct microporous structure (around 1 nm) within the HPSs. The microporous structure of PCNs and N-PCNs is not readily apparent, resulting in a reduction of the Bruner–Emmet–Teller surface area (SBET) from 279.71 $m^2 \cdot g^{-1}$ (HPSs) to 31.23 and 41.41 $m^2 \cdot g^{-1}$, respectively, which may be attributed to the blockage of pores by volatile and carbonaceous products generated during thermal decomposition (Fig. 2(i) and Table S2 in the ESM) [38]. The N_2 adsorption/desorption curves in Fig. 2(i), F,N,S-PCNs indicate a rapid increase in N_2 adsorption at relative pressure P/P_0 = 0–0.1, suggesting the presence of a substantial micropore structure with the primary pore size distribution ranging from 0.5 to 0.8 nm. SBET of F,N,S-PCNs has increased to 398.57 $m^2 \cdot g^{-1}$, providing further evidence that the PDA-NTf_2 coating layer on the

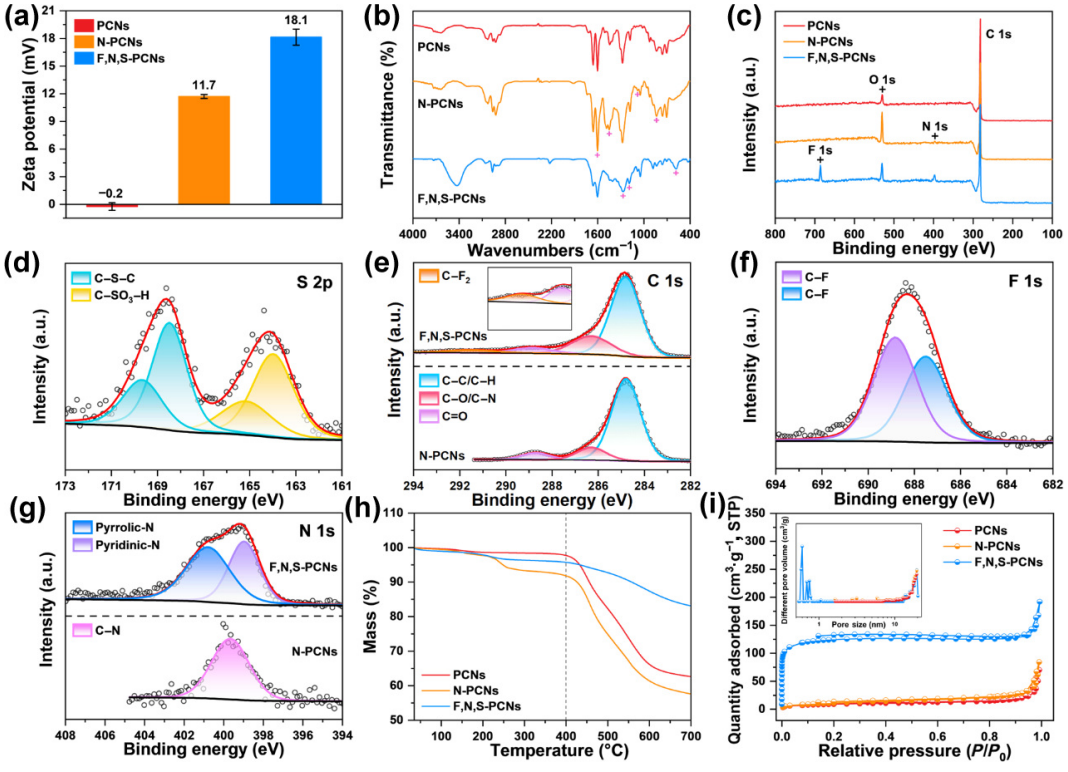

Figure 2 (a) Zeta-potential, (b) FT-IR spectra, (c) full XPS spectra, (h) TG curves, and (i) BET and the corresponding pore size distribution curves of samples. (d) S 2p, (e) C 1s, (f) F 1s, and (g) N 1s XPS fine spectra of samples.

nanospheres has completely disintegrated and that F,N,S doping has introduced a substantial number of microscopic pores into the nanosphere.

Nanospheres exhibit a high surface energy, leading to a pronounced tendency for agglomeration, which significantly limits their compatibility with dispersants. Based on Fig. S7 in the ESM, following a 48-hour exposure to room temperature, the 500SN + PCNs and 500SN + N-PCNs displayed observable layering phenomenon, while the 500SN + F,N,S-PCNs exhibited sustained dispersibility stability. In these experiments, nanospheres were utilized at different concentrations (1.0 wt.%–3.0 wt.%) under constant conditions (150 N, 25 Hz, 50 °C) to determine the optimal concentration for enhanced efficacy. Based on Fig. 3(a) and Fig. S8 in the ESM, the COF of the nanolubricant (500SN + 2.0 wt.% F,N,S-PCNs) decrease from 0.146 to 0.110 and a reduction in wear volume (5.0×10^4 μm^3) by 41.5% compared to 500SN + 1.0 wt.% F,N,S-PCNs. When the addition amount exceeds 2.0 wt.%, there is a slight increase in the COF (0.115) and wear volume (5.3×10^4 μm^3) of 500SN + 3.0 wt.% F,N,S-PCNs. This phenomenon can be attributed to the fact that at concentration of 2.0 wt.% F,N,S-PCNs, the nanospheres in the contact area have already reached saturation, rendering further increases in additive concentration ineffective in enhancing lubrication [39]. The COF and wear volume of 500SN, PCNs, N-PCNs and F,N,S-PCNs based lubricant (with a 2.0 wt.% addition) are presented in Figs. 3(b) and 3(c). Prior to 250 s, there was a marked increase in the COF of 500SN, 500SN + PCNs, and 500SN + N-PCNs to 0.360, 0.296, and 0.216 respectively. The mean COF of nanolubricant (500SN + F,N,S-PCNs) resulted in a significant reduction to 0.110, representing a decrease of 39.2%, 35.0%, and 31.7% compared to 500SN (0.181), PCNs (0.169), and N-PCNs (0.161) respectively. The wear volume of F,N,S-PCNs was reduced to 5.0×10^4 μm^3, compared to 500SN (5.2×10^5 μm^3), PCNs (9.8×10^4 μm^3), and N-PCNs (1.27×10^5 μm^3), respectively, resulting in reductions of 90.3%, 49.0%, and 60.6%.

Figures 3(d)–3(f) illustrate an in-depth analysis of the tribological behavior of different nanolubricant under extreme operating conditions. Under high-pressure conditions, the load-carrying capacity of F,N,S-PCNs as lubricant additives is enhanced from 150 N (500SN) to 450 N. Under variable frequency conditions, the mean COF of 500SN + F,N,S-PCNs was reduced to 0.141 compared to that of 500SN (0.169), 500SN + PCNs(0.167), and 500SN + N-PCNs (0.165). Under varying temperature conditions, the COF of 500SN, 500SN + PCNs, and 500SN + N-PCNs increased to 0.60 (40 °C), 0.21 (50 °C), and 0.20 (40 °C) respectively. 500SN + F,N,S-PCNs demonstrated excellent high-temperature resistance at temperatures below 70 °C, maintaining a COF of 0.12 or lower. Hence, F,N,S-PCNs as nano-additives manifest exceptional wear resistance and friction reduction properties, and demonstrate good lubricating performance in extreme operating conditions.

The wear process involves the continuous removal of a friction pair's surface layer during relative motion, which is an inevitable consequence of friction. Figure 4 illustrates the SEM images, as well as the 3D profile morphology and its corresponding cross-sectional wear morphology. As depicted in Fig. 4(a), the surface lubricated with 500SN displayed irregular topography, with wear depth of 4.3 μm and wear area of 600.9 μm^2, which is due to the formation of adhesion points resulting in severe wear on the friction pair surface. When PCNs and N-PCNs are utilized as lubricant additives, adhesive wear still occurs on the contact surface (Figs. 4(b) and 4(c)). However, owing to the nanospheres' size effect, they can infiltrate the clearance between the friction pairs and adhere to the surface, thereby diminishing surface roughness and preventing direct contact between the friction pairs, ultimately mitigating damage. Hence, wear depth lubricated with 500SN + 2.0 wt.% PCNs and 500SN + 2.0 wt.% N-PCNs is 2.4 and 3.6 μm, respectively, accompanied by wear area measuring 118.2 and 210.3 μm^2. Microgrooves develop on the worn surface lubricated by 500SN + 2.0 wt.% F,N,S-PCNs in the direction of friction due to abrasive wear, accompanied by wear depth and wear area of 0.77 μm and 47.7 μm^2, respectively (Fig. 4(d)). As shown in Fig. S9 in the ESM, the mapping energy spectrum of the wear spot exhibited an uneven distribution of C, N, O, and S, which could be ascribed to the adsorption of F,N,S-PCNs on the friction pair surface, forming the deposition film, and the occurrence of frictional chemical reactions between the active elements (F,N,S) in the F,N,S-PCNs and the friction pair (generating the chemical protective film). The creation of the composite protective film (consisting of the deposition film and chemical protective film) prevents direct contact between the friction pair, leading to significant reductions in both friction and wear. Hence, F,N,S-

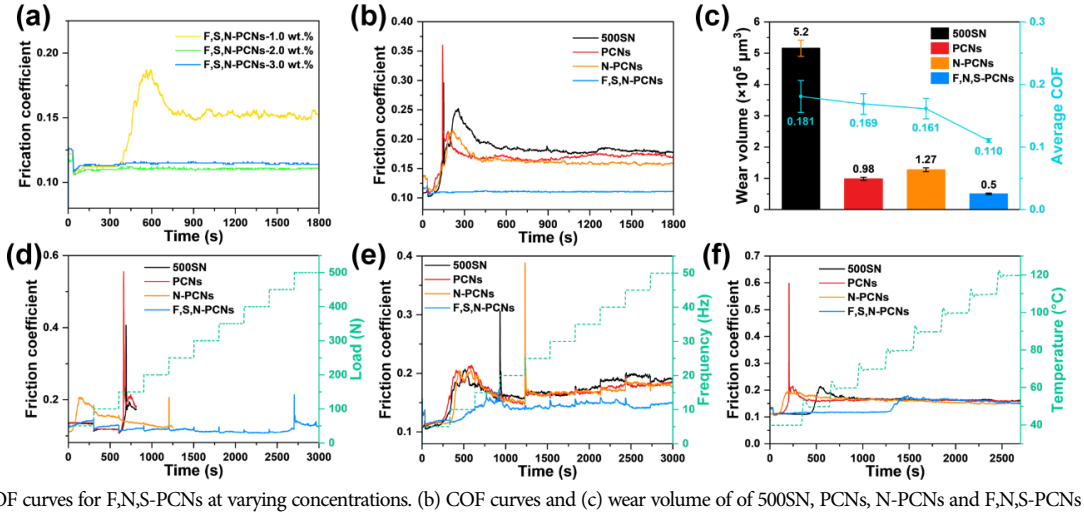

Figure 3 (a) COF curves for F,N,S-PCNs at varying concentrations. (b) COF curves and (c) wear volume of of 500SN, PCNs, N-PCNs and F,N,S-PCNs based lubricant (with a 2.0 wt.% addition). The COF evolution curves for various lubricants under (d) high pressure, (e) different frequency, and (f) different temperature.

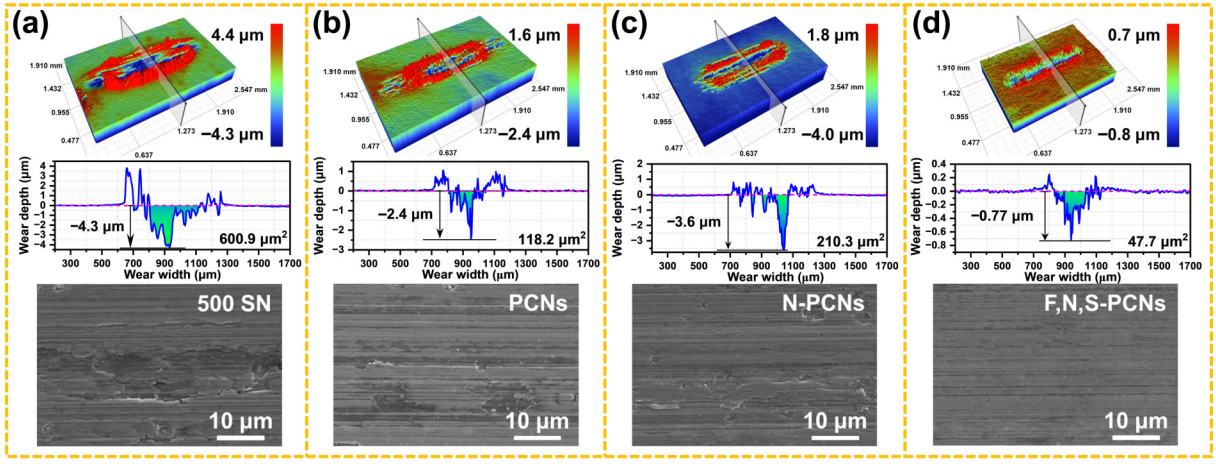

Figure 4 SEM images, wear depth, wear area, and the three-dimensional optical microscopic morphology of worn surfaces based (a) 500SN, (b) PCNs, (c) N-PCNs, and (d) F,N,S-PCNs.

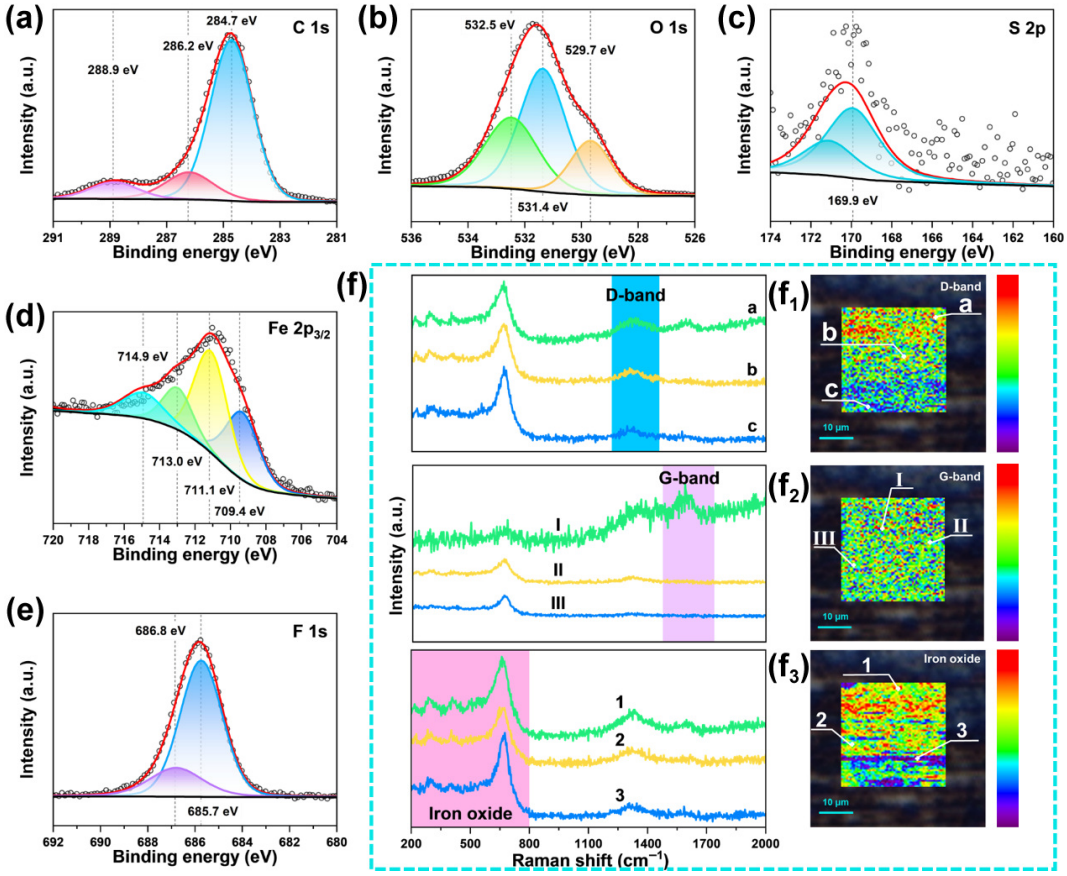

Figure 5 XPS fine spectra ((a) C 1s, (b) O 1s, (c) S 2p, (d) Fe $2p_{3/2}$, and (e) F 1s) of wear scar based 500SN + 2.0 wt.% F,N,S-PCNs. (f) The intensity mapping of Raman spectra on the worn surface lubricated by 500SN + 2.0 wt.% F,N,S-PCNs.

PCNs as lubricant additives can effectively reduce the depth and area of wear, prevent adhesive wear, and achieve significant anti-wear effects.

The chemical state of the worn surface was analyzed using XPS and Raman, as depicted in Fig. 5 and Fig. S10 in the ESM, to investigate the anti-friction and anti-wear mechanism. The C 1s spectra exhibit distinct peaks at 284.7 eV for C–C, 286.3 eV for C–O, and 288.8 eV for C=O, respectively, corresponding with the O 1s spectra (531.4 eV (C=O), 532.5 eV (C–O)), indicating the deposition of carbon nanospheres on the worn surfaces (Figs. 5(a) and 5(b)). The N 1s spectra is illustrated in Fig. S10 in the ESM, with the pyrrolic-N peak discerned at 400.4 eV. The S $2p_{3/2}$ spectra (Fig. 5(c)) exhibit a prominent SOF_2 signal at 169.9 eV [40]. As illustrated in Fig. 5(d), the Fe $2p_{3/2}$ spectra exhibit distinct peaks corresponding to FeO at 709.4 eV, FeOOH at 711.1 eV, Fe_2O_3 at 713.0 eV, and FeF_3 at 714.9 eV, respectively, corresponding with the O 1s (529.7 eV (metal oxide)) and F 1s (686.8 eV (metal fluoride)) spectra [41, 42]. The peak at 685.7 eV (C–F) suggests the deposition of F,N,S-PCNs on the friction pair surface (Fig. 5(e)) [43]. The composition of the protective film was additionally examined

through Raman spectroscopy, as shown in Fig. 5(f). In Fig. 5(f_1), depicts the intensity map of the D band (1350 cm^{-1}) is illustrated by a predominantly bright color, indicative of high signal intensity and extensive coverage. Analysis of three points in different color regions reveals the presence of both the D band and G band in area with varying intensities, indicating deposition of F,N,S-PCNs on the friction pair's surface (Fig. S11 in the ESM) [44]. Additionally, characteristic peaks for iron oxide are observed in the range of 200 to 600 cm^{-1} (Fig. 5(f_3)), suggesting the formation of a friction film comprising carbon compounds and iron oxides on the wear trace. In contrast, Fig. 5(f_2)'s intensity map for the G band (1580 cm^{-1}) shows significantly weaker signal intensity, dominated by green hues with an absence of G bands in purple or green regions. The intensity maps for both D and G bands indicate that most carbon-containing compounds in the friction film are amorphous. Consequently, F,N,S-PCNs as additives can adsorb onto the surface of the friction pair to form a physical deposit film, while F,N,S-PCNs can undergo chemical reactions with the friction pair to create a chemical protective film containing sulfides, iron oxides, metal fluorides, and carbon nitrides.

Therefore, Scheme 2 illustrates the friction mechanism of F,N,S-PCNs as lubricant additives. Due to the small size effect, nanospheres are able to penetrate the gap between the friction pair and adsorb onto the surface, thereby preventing direct contact between the friction pair (adsorption effect). Some of the nanospheres fill in the depressions on the friction pair, surface, reducing surface roughness (mending effect). Additionally, nanospheres that are adsorbed onto the friction pair form a physical adsorption film, which undergoes chemical reactions with the friction pair under mechanical force and heat to produce a protective film composed of metal oxides, metal fluorides, sulfur-containing compounds, and carbon nitride compounds (chemical protective film). Through these mechanisms including mending effect, adsorption effect, and chemical protective film, effective lubrication and wear resistance are achieved.

4 Conclusion

In this study, a compact and stable PDA coating was fabricated on HPSs using PEI as a crosslinking agent. After acidification treatment, anionic exchange with $LiNTf_2$ was performed, thereby yielding HPSs@PDA-NTf_2. By means of the carbonization at high-temperature, F,N,S-PCNs were fabricated. The tribological performance of F,N,S-PCNs as a lubricant additive was thoroughly analyzed under various condition. The experiment result indicate that, compared to 500SN, the mean COF of nanolubricant (500SN + F,N,S-PCNs) decreases to 0.11, resulting in a reduction of wear volume by 90.3%, accompanied by a significant reduction in wear width (82.1%) and wear area (92.1%). Due to the small size effect, F,N,S-PCNs are able to penetrate the gap between friction pairs and adsorb onto the surface, forming a physical adsorption film to prevent direct contact of friction pair. Additionally, these nanoparticles undergo chemical reactions on friction pair surfaces, generating a chemical protective film including metal oxides, metal fluorides, sulfur-containing compounds, and nitrogen-carbon compounds. The composite protective film, comprising a deposition film and a chemical protective film, significantly improve their tribological performance and anti-wear characteristics. The novel method offers a groundbreaking approach to fabricate carbon nanospheres doped with multiple elements, enabling precise control over the doping process. Its efficiency, controllability, and reproducibility open new avenues for developing high-performance carbon materials with versatile applications.

Electronic Supplementary Material: Supplementary material (SEM, zeta-potential, FT-IR spectra, full XPS spectrum, BET and the corresponding pore size distribution curves of samples, and the wear volume of lower disks lubricated by 500SN with F,N,S-PCNs) is available in the online version of this article at https://doi.org/10.26599/NR.2025.94906995.

Data availability

All data needed to support the conclusions in the paper are presented in the manuscript and the Electronic Supplementary Material. Additional data related to this paper may be requested from the corresponding author upon request.

Acknowledgement

This work was supported by the National Natural Science Foundation of China (Nos. U23A20623 and U21A2046), the

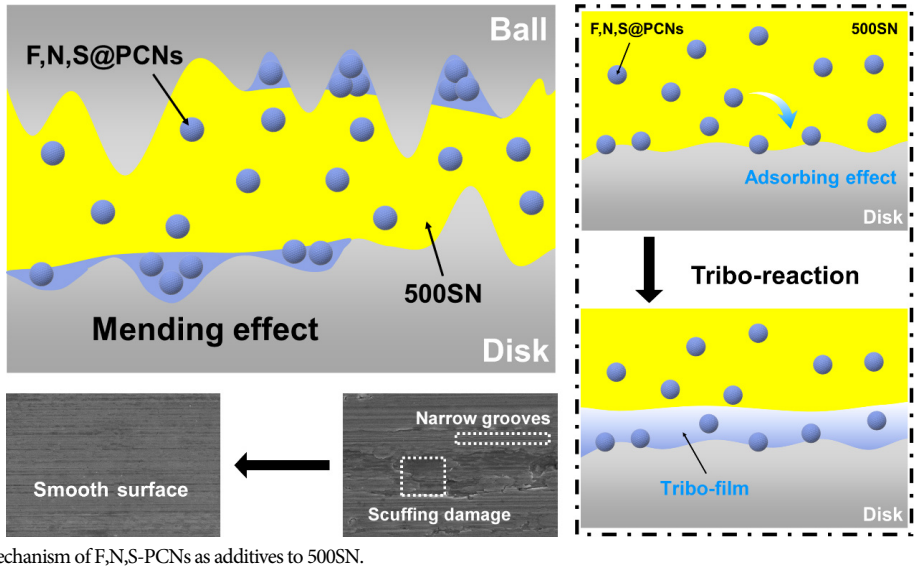

Scheme 2 Lubrication mechanism of F,N,S-PCNs as additives to 500SN.

Western Light Project of CAS (No. xbzg-zdsys-202118), Shaanxi Provincial Science and Technology Innovation Team (No. 2024RS-CXTD-63), and the Research Fund of the State Key Laboratory of Solidification Processing (NPU), China (No. 2023-TS-03).

Declaration of competing interest

The authors declare that they have no known competing financial interests or personal relationships that could have appeared to influence the work reported in this paper.

Author contribution statement

Y. X. W.: Writing – original draft, formal analysis, data curation. Y. W.: Investigation. Y. H. C.: Data curation. S. L.: Data curation. S. J. L.: Writing – review & editing. Q. Y.: Supervision, writing – review & editing. F. Z.: Supervision, writing – review & editing. W. M. L.: Supervision, writing – review & editing.

Use of AI statement

None.

References

[1] Cui, Y. H.; He, B. L.; Xue, S. H.; Chen, Z.; Liu, S. J.; Ye, Q.; Zhou, F.; Liu, W. M. Fabrication of MXene@Fe_3O_4@PNA composite with photothermal effect as water-based lubricant additive. *Chem. Eng. J.* **2023**, *469*, 143880.

[2] Wang, K. P.; Liu, L.; Song, A. S.; Ma, T. B.; Wang, H. D.; Luo, J. B.; Liu, Y. H. Macroscale superlubricity under ultrahigh contact pressure in the presence of layered double hydroxide nanosheets. *Nano Res.* **2022**, *15*, 4700–4709.

[3] Liu, S. W.; Gao, Q. L.; Hou, K. M.; Li, Z. P.; Wang, J. Q.; Yang, S. R. Solvent-free covalent, MXene nanofluid: A new lubricant combining the characteristics of solid and liquid lubricants. *Chem. Eng. J.* **2023**, *462*, 142238.

[4] Wang, S. Y.; Chen, D.; Hong, Q.; Gui, Y.; Cao, Y. C.; Ren, G. L.; Liang, Z. Surface functionalization of metal and metal oxide nanoparticles for dispersion and tribological applications—A review. *J. Mol. Liq.* **2023**, *389*, 122821.

[5] Du, F. M.; Li, C.; Li, D. W.; Sa, X. X.; Yu, Y.; Li, C. D.; Yang, Y. X.; Wang, J. L. Research progress regarding the use of metal and metal oxide nanoparticles as lubricant additives. *Lubricants* **2022**, *10*, 196.

[6] Fan, X. Q.; Li, X. P.; Zhao, Z.; Yue, Z. F.; Feng, P.; Ma, X. L.; Li, H.; Ye, X. Y.; Zhu, M. H. Heterostructured rGO/MoS_2 nanocomposites toward enhancing lubrication function of industrial gear oils. *Carbon* **2022**, *191*, 84–97.

[7] Cui, Y. H.; Xue, S. H.; Wang, S. Y.; Chen, X.; Liu, S. J.; Ye, Q.; Zhou, F.; Liu, W. M. Fabrication of carbon dots intercalated MXene hybrids via laser treatment as oil-based additives for synergistic lubrication. *Carbon* **2023**, *205*, 373–382.

[8] Gong, H. J.; Song, Y.; Li, G. L.; Zhang, L.; Guo, D.; Xie, G. X. An intelligent polymer composite with self-lubricating and self-healing functionalities. *Compos. B Eng.* **2023**, *260*, 110776.

[9] Gulzar, M.; Masjuki, H. H.; Kalam, M. A.; Varman, M.; Zulkifli, N. W. M.; Mufti, R. A.; Zahid, R. Tribological performance of nanoparticles as lubricating oil additives. *J. Nanopart. Res.* **2016**, *18*, 223.

[10] Liu, J. M.; Chen, B. B.; Guo, P. L.; Yu, Z. Q.; Sheng, W. C.; Zhang, K.; Liu, X. Q. Fabrication of 3D porous graphene materials for oil-based lubrication: Tribological and wear performance. *Carbon* **2024**, *221*, 118892.

[11] Wang, S. Y.; Ren, G. L.; Li, W. Q.; Wang, B.; Wei, F. H.; Liang, Z.; Chen, D. A green modification technology of carbon nanotubes toward enhancing the tribological properties of aqueous-based lubricants. *Tribol. Int.* **2023**, *180*, 108268.

[12] Piya, A. K.; Yang, L.; Omar, A. A. S.; Emami, N.; Morina, A. Synergistic lubrication mechanism of nanodiamonds with organic friction modifier. *Carbon* **2024**, *218*, 118742.

[13] Liu, S.; Wang, Y. X.; Zhang, X. Z.; Liu, S. J.; Ye, Q.; Liu, W. M. Sulfur-containing carbon nanospheres as lubricant additives for antiwear and friction reduction. *ACS Appl. Nano Mater.* **2023**, *6*, 18539–18547.

[14] Zhai, W. Z.; Srikanth, N.; Kong, L. B.; Zhou, K. Carbon nanomaterials in tribology. *Carbon* **2017**, *119*, 150–171.

[15] Tan, S. C.; Shi, H. Y.; Du, X.; Wang, K. P.; Xu, H. J.; Wan, J. H.; Deng, K.; Zeng, Q. D.; Liu, Y. H. Electric field controlled superlubricity of fullerene-based host-guest assembly. *Nano Res.* **2023**, *16*, 583–588.

[16] Büch, H.; Rossi, A.; Forti, S.; Convertino, D.; Tozzini, V.; Coletti, C. Superlubricity of epitaxial monolayer WS_2 on graphene. *Nano Res.* **2018**, *11*, 5946–5956.

[17] Zhang, Y. P.; Jia, X. H.; Tian, Q.; Yang, J.; Wang, S. Z.; Li, Y.; Shao, D.; Feng, L.; Song, H. J. Synthetic kilogram carbon dots for superior friction reduction and antiwear additives. *Langmuir* **2022**, *38*, 7791–7801.

[18] Nyholm, N.; Espallargas, N. Functionalized carbon nanostructures as lubricant additives—A review. *Carbon* **2023**, *201*, 1200–1228.

[19] Chen, X. C.; Li, J. J. Superlubricity of carbon nanostructures. *Carbon* **2020**, *158*, 1–23.

[20] Wang, H.; Shao, Y.; Mei, S. L.; Lu, Y.; Zhang, M.; Sun, J. K.; Matyjaszewski, K.; Antonietti, M.; Yuan, J. Y. Polymer-derived heteroatom-doped porous carbon materials. *Chem. Rev.* **2020**, *120*, 9363–9419.

[21] Zahid, R.; Masjuki, H. H.; Varman, M.; Mufti, R. A.; Kalam, M. A.; Gulzar, M. Effect of lubricant formulations on the tribological performance of self-mated doped DLC contacts: A review. *Tribol. Lett.* **2015**, *58*, 32.

[22] Jin, G. K.; Xue, S. H.; Zhang, R.; Liu, S.; Wang, S. Y.; Liu, S. J.; Ye, Q.; Wang, H. Q.; Zhou, F.; Liu, W. M. Pulsed laser manufactured heteroatom doped carbon dots via heterocyclic aromatic hydrocarbons for improved tribology performance. *Small* **2024**, *20*, 2311876.

[23] Wang, F.; Wang, L. P.; Xue, Q. J. Fluorine and sulfur co-doped amorphous carbon films to achieve ultra-low friction under high vacuum. *Carbon* **2016**, *96*, 411–420.

[24] Gong, J.; Chen, X. C.; Tang, T. Recent progress in controlled carbonization of (waste) polymers. *Prog. Polym. Sci.* **2019**, *94*, 1–32.

[25] Yang, S. J.; Zou, L. Y.; Liu, C.; Zhong, Q.; Ma, Z. Y.; Yang, J.; Ji, J.; Müller-Buschbaum, P.; Xu, Z. K. Codeposition of levodopa and polyethyleneimine: Reaction mechanism and coating construction. *ACS Appl. Mater. Interfaces* **2020**, *12*, 54094–54103.

[26] Liu, Y. L.; Ai, K. L.; Lu, L. H. Polydopamine and its derivative materials: Synthesis and promising applications in energy, environmental, and biomedical fields. *Chem. Rev.* **2014**, *114*, 5057–5115.

[27] Poinard, B.; Kamaluddin, S.; Tan, A. Q. Q.; Neoh, K. G.; Kah, J. C. Y. Polydopamine coating enhances mucopenetration and cell uptake of nanoparticles. *ACS Appl. Mater. Interfaces* **2019**, *11*, 4777–4789.

[28] Mou, Z. H.; Peng, J.; Yan, R. X.; Li, Y.; Zhao, B.; Wang, Z. J.; Xiao, D. Synthesis of polyelectrolyte-decorated polydopamine nanoparticles via surface reconstruction for enhancing oil-based lubrication. *Chem. Eng. J.* **2024**, *480*, 147959.

[29] Wang, Y. X.; Zhang, T. T.; Qiu, Y. Q.; Guo, R. S.; Xu, F.; Liu, S. J.; Ye, Q.; Zhou, F. Nitrogen-doped porous carbon nanospheres derived from hyper-crosslinked polystyrene as lubricant additives for friction and wear reduction. *Tribol. Int.* **2022**, *169*, 107458.

[30] Rezaii, E.; Mahkam, M.; Assadi, M. G.; Dolati, H. A facile synthesis

of nitrogen-doped bamboo-shaped carbon nanotubes by catalytic decomposition of 2-aminopyrimidine over Fe@MgO catalyst through chemical vapor deposition method. *Chem. Pap.* **2021**, *75*, 591–598.

[31] Chen, W. J.; Zhang, K. F.; Xu, C. H.; Zhang, F.; Du, L. Preparation of MDEA derived nitrogen-doped CQDs nanofluids and their CO_2 capturing performance and mechanism investigation. *Sep. Purif. Technol.* **2024**, *334*, 126049.

[32] Atchudan, R.; Edison, T. N. J. I.; Perumal, S.; Lee, Y. R. Green synthesis of nitrogen-doped graphitic carbon sheets with use of *Prunus persica* for supercapacitor applications. *Appl. Surf. Sci.* **2017**, *393*, 276–286.

[33] Li, Q. F.; Liu, S. R.; Zhang, X.; Hu, G. S.; Xia, H. A. High-efficiency sulfur-doped carbon photocatalysts synthesized by carbonization of lignosulfonate at low temperature. *Mater. Today Commun.* **2022**, *33*, 104448.

[34] Xue, S. H.; Cui, Y. H.; Jin, G. K.; Wang, H. Y.; Liu, S. J.; Ye, Q.; Wang, H. Q.; Zhou, F.; Liu, W. M. Carbon dots with spatially-mediated-N/S-Co-doping enabling one-year stable lubricant with oil leakage detection capability. *Small* **2024**, *20*, 2312010.

[35] Li, G. F.; Yang, F.; Wu, L. S.; Qian, L.; Hu, X. R.; Wang, Z. M.; Chen, W. Agricultural waste buckwheat husk derived bifunctional nitrogen, sulfur and oxygen-co-doped porous carbon for symmetric supercapacitors and capacitive deionization. *New J. Chem.* **2021**, *45*, 10432–10447.

[36] Wang, Y. X.; Liu, S.; Cui, Y. H.; Bai, W.; Liu, S. J.; Ye, Q.; Zhou, F.; Liu, W. M. *In-situ* pyrolysis synthesis of multi-element (F, N, S) co-doped porous carbon nanospheres as lubricating additives with improved tribological behaviors. *Carbon* **2024**, *218*, 118724.

[37] Shulga, Y. M.; Tien, T. C.; Huang, C. C.; Lo, S. C.; Muradyan, V. E.; Polyakova, N. V.; Ling, Y. C.; Loutfy, R. O.; Moravsky, A. P. XPS study of fluorinated carbon multi-walled nanotubes. *J. Electron Spectrosc. Relat. Phenom.* **2007**, *160*, 22–28.

[38] Zeng, X. Y.; Wang, Y.; Li, R. X.; Cao, H. L.; Li, Y. F.; Lü, J. Impacts of temperatures and phosphoric-acid modification to the physicochemical properties of biochar for excellent sulfadiazine adsorption. *Biochar* **2022**, *4*, 14.

[39] Alazemi, A. A.; Etacheri, V.; Dysart, A. D.; Stacke, L. E.; Pol, V. G.; Sadeghi, F. Ultrasmooth submicrometer carbon spheres as lubricant additives for friction and wear reduction. *ACS Appl. Mater. Interfaces* **2015**, *7*, 5514–5521.

[40] Lindberg, B. J.; Hamrin, K.; Johansson, G.; Gelius, U.; Fahlman, A.; Nordling, C.; Siegbahn, K. Molecular spectroscopy by means of esca II. Sulfur compounds. Correlation of electron binding energy with structure. *Phys. Scr.* **1970**, *1*, 286–298.

[41] Carver, J. C.; Schweitzer, G. K.; Carlson, T. A. Use of X-ray photoelectron spectroscopy to study bonding in Cr, Mn, Fe, and Co compounds. *J. Chem. Phys.* **1972**, *57*, 973–982.

[42] Nefedov, V. I.; Salyn, Y. V.; Sadovsky, A. P.; Beyer, L. The structure of the valence levels of iron nitrosyls from the X-ray photoelectron and X-ray spectra. *J. Electron Spectrosc. Relat. Phenom.* **1977**, *12*, 121–132.

[43] Zhang, R. H.; Shen, M. X.; He, Z. Y. The unusual tribological behavior of diamond-like carbon films under high vacuum. *Surf. Interface Anal.* **2020**, *52*, 339–347.

[44] Lu, Q.; Zhang, T. Y.; Wang, Y. X.; Liu, S. J.; Ye, Q.; Zhou, F. Boron-nitrogen codoped carbon nanosheets as oil-based lubricant additives for antioxidation, antiwear, and friction reduction. *ACS Sustain. Chem. Eng.* **2023**, *11*, 11867–11877.